Article

Journal of
Biomedical Nanotechnology
Vol. 12, 1916–1928, 2016
www.aspbs.com/jbn

Construction of 3-D Cellular Multi-Layers with Extracellular Matrix Assembly Using Magnetic Nanoparticles

Yu Bin Lee[1, 2, †], Joong-Yup Lee[1, 2, †], Taufiq Ahmad[1, 2], Seongwoo Bak[1, 2], Jinkyu Lee[1, 2], Hwan D. Kim[3], Tai Hyun Park[3, 4], Nathaniel S. Hwang[3], Youn Mook Lim[5, *], and Heungsoo Shin[1, 2, *]

[1] *Department of Bioengineering, Institute for Bioengineering and Biopharmaceutical Research, Hanyang University, Seoul, 133-791, Republic of Korea*
[2] *BK21 Plus Future Biopharmaceutical Human Resources Training and Research Team, Hanyang University, Seoul, 133-791, Republic of Korea*
[3] *School of Chemical and Biological Engineering, Seoul National University, Seoul, 151-742, Republic of Korea*
[4] *Advanced Institutes of Convergence Technology, Suwon 443-270, Republic of Korea*
[5] *Research Division for Industry and Environment, Advanced Radiation Technology Institute, Korea Atomic Energy Research Institute, 29 Gumgugil, Jeongeup, Jeollabuk-do 580-185, Republic of Korea*

Construction of 3-dimensional (3-D) engineered tissue is increasingly being investigated for use in drug discovery and regenerative medicine. Here, we developed multi-layered 3-D cellular assembly by using magnetic nanoparticles (MNP) isolated from *Magnetospirillum* sp. AMB-1 magnetotactic bacteria. Magnetized human dermal fibroblasts (HDFBs) were prepared by treatment with the MNP, induced to form 3-D assembly under a magnetic field. Analyses including LIVE/DEAD assay, transmission electron microscopy revealed that the MNP were internalized via clathrin-mediated endocytosis without cytotoxicity. The magnetized HDFBs could build 3-D structure as a function of seeding density. When the highest seeding density (5×10^5 cells/mm^2) was used, the thickness of assembly was 41.90 ± 1.69 μm, with approximately 9.3 ± 1.6 cell layers being formed. Immunofluorescence staining confirmed homogeneous distribution of ECM and junction proteins throughout the 3-D assembly. Real-time PCR analysis showed decrease in expression levels of collagen types I and IV but increase in that of connexin 43 in the 3-D assembly compared with the 2-D culture. Finally, we demonstrated that the discernible layers can be formed hierarchically by serial assembly. In conclusion, our study showed that a multi-layered structure can be easily prepared using magnetically-assisted cellular assembly with highlighting cell-cell and cell-ECM communication.

KEYWORDS: *Hierarchical Tissue Mimicry, Multi-Layered Structure, 3-D Cellular Assembly, Magnetic Nanoparticles, Cellular Internalization.*

INTRODUCTION

Human tissue is composed of multiple cell types and extracellular matrix (ECM) molecules that are hierarchically integrated to form a complex three-dimensional (3-D) structure. Biological cues derived from cell-cell communication, cell-ECM binding, biochemical signaling, and mechanical forces collectively regulate many critical functions of tissue.[1] Engineering sophisticated 3-D tissue is increasingly being investigated not only as a cell culture model alternative to the conventional 2-D system, but also as a therapeutic source to replace damaged tissue in regenerative medicine.[2–4] Complex structure of 3-D tissue has been recapitulated through either top-down or bottom-up approaches. Top-down approaches involve biomaterial scaffolds, on which cells are attached, proliferating and differentiated to form multi-scale structure dictating 3-D shapes of underlying scaffolds.[5] In contrast, the bottom-up approach considers multiple cell types as constructive units that are processed and engineered to be assembled to

*Authors to whom correspondence should be addressed.
Emails: ymlim71@kaeri.re.kr, hshin@hanyang.ac.kr
†These two authors contributed equally to this work
Received: 17 March 2016
Revised/Accepted: 1 June 2016

 1550-7033/2016/12/1916/013 doi:10.1166/jbn.2016.2303

establish a 3-D architecture, mainly via self-assembly of individual cells.[6]

One of the popular 3-D structures engineered by a bottom-up approach is spheroid fabricated with many sizes and functions depending on the number and type of cells.[7] However, it is often impossible to control the organization of multiple cell types, the spheroid structure is not well reproducible, and hypoxia within the spheroid causes cell death.[8] Cell sheet engineering uses thermoresponsive cell culture plates that allow the cell layer to be harvested without using proteolytic enzymes. The resulting cell sheet is retained under the ECM and allows serially-stacked cell sheets to form multilayered 3-D engineered tissue.[9] On the other hand, the cell accumulation technique uses similar interactions between cells and the ECM. In this approach, cells are coated with a nanometer film that consists of layer-by-layer assembled fibronectin and gelatin, which drive spontaneous formation of cell-to-cell aggregates.[10] Although these techniques enable us to facilitate 3-D tissue construction with multiple cell types, requirement of labor-intensive works and resulting long processing time would be problematic.

An additional promising bottom-up approach involves magnetic force-assisted cellular assembly.[11] In this process, cells are incubated with magnetic nanoparticles and the magnetized cells are then be assembled onto the surface of a culture dish or levitated from the bottom surface to form a 3-D cell aggregate, depending on the placement of the applied external magnetic field.[12–14] The magnetic-based 3-D cell aggregation has been demonstrated with many cell types such as fibroblasts, endothelial cells, hepatocytes, adipocytes, keratinocytes, mesenchymal stem cells (hMSCs), and induced pluripotent stem cells for either *in vitro* culture models or *in vivo* animal models.[15–19] The feasibility of co-culture by assembling different cell types and a unique cell arrangement via a controlled magnetic field was also investigated.[20] Recently, our colleagues reported the use of ferromagnetic nanoparticles (MNP) isolated from a strain of magnetotactic bacteria, *Magnetospirillum* sp. AMB-1, for levitation of hMSCs as a form of 3-D spheres with a multi-compartment structure.[21,22] Compared to previously studied systems, these MNP were efficiently delivered into the cytoplasm with no requirement of further modification with positively-charged molecules. However, the underlying principle of MNP internalization, controllability of multi-layered 3-D assembled structure formation, and cell-cell/cell-ECM interactions within the 3-D assembly have not yet been fully investigated.

The purpose of study was to achieve fine control of magnetically-assisted magnetized cell assembly with multi-layered architecture. We first investigated the effect of MNP concentration on internalization to human dermal fibroblasts (HDFBs) and studied the underlying endocytosis mechanism. We then examined 3-D assembly formation to illustrate the feasibility of multi-layered structure control by adjusting the cell number. The effect of magnetically-assisted 3-D assembly on the expression of ECM and cell junction proteins was also analyzed. Finally, we confirmed the construction of a clearly separated, three-layered structure via serial assembly of magnetized cells.

EXPERIMENTAL DETAILS

Magnetic Nanoparticles (MNP) Preparation

Ferromagnetic iron oxide (Fe_3O_4) nanoparticles (herein, referred as MNP) were isolated from *Magnetospirillum*sp. AMB-1 as previously described.[21] The bacteria were cultured in magnetic spirillum growth medium for 5 days at 27 °C under anaerobic conditions. After purification, MNP were concentrated to 1 mg/ml in PBS and stored at 4 °C and fully re-dispersed using a bath sonicator (JAC 1505, Korea) for 15 min prior to use.

In Vitro Cell Culture and Characterization of MNP Internalization

HDFBs (Lonza, Carlsbad, CA, USA) were cultured in high glucose Dulbecco's modified Eagle's medium (DMEM) with 10% FBS and 1% penicillin/streptomycin at standard culture conditions (95% humidity, 37 °C and 5% CO2). To study the cellular uptake of MNP, HDFBs were detached using Trypsin-EDTA, re-seeded on a 24-well tissue culture plate in a density of 1×10^4 cells/cm^2, and incubated for 12 hrs. The medium was then replenished with different amounts of MNP (1 to 3 μg/cm^2), and the cell culture was maintained for an additional 24 hrs. Magnetized cells were then visualized by combining Prussian blue staining and hematoxylin staining. Briefly, the cells were fixed with 4% paraformaldehyde for 20 min at 4 °C and gently washed with PBS. We then added a 1:1 mixture of aqueous solution of potassium ferrocyanide (10% w/v) and an aqueous hydrochloric acid solution (20% w/v) to each well for 20 min. Mayor's hematoxylin was then treated for 1 hr. Iron assay kit (Biovision Research, Milpitas, CA, USA) was used for quantification of the incorporated amount of MNP. HDFBs treated with different concentrations of MNP were lysed using 150 μl of a 0.1% SDS solution, 50 μl of the cell lysate was collected and mixed with 50 μl of the iron assay buffer in a 96-well plate. Next, 5 μl of reducer was added to each well for 30 min, followed by addition and incubation with 100 μl of iron probe for 1 hr. The optical density was measured by a spectrometer (Spectra Max M2E, Molecular Devices, CA, USA) at 593 nm. Iron content in each cell was calculated to divide measured iron by the total cell number in each well. The internalized MNP were visualized using transmission electron microscopy (TEM) (LIBRA 120, Carl Ziess, Germany). HDFBs treated with MNP (2 μg/cm^2) were centrifuged and fixed with modified Karnovky's fixative solution (2% paraformaldehyde and 2% glutaraldehyde in 0.05 M sodium cacodylate buffer, pH 7.2) and 1% osmium tetroxide (in 0.05 M sodium cacodylate buffer, pH 7.2).

The fixed cells were serially dehydrated with different concentrations of ethanol (EtOH) (30 to 100%). The transition step was performed with 100% propylene oxide at room temperature for 15 min, and the samples were then embedded with Spurr's resin at 70 °C for 24 hrs. The polymerized Spurr's resin blocks were sectioned with an ultra microtome (MT-X, RMC, Tucson, AZ, USA) and stained with 2% uranyl acetate and Reynolds' Lead citrate for 7 min.

MNP Uptake Cytotoxicity

After exposure to MNP for 1 day, HDFBs were treated with a LIVE/DEAD® assay (Invitrogen, Carlsbad, CA, USA) solution (0.1% calcein AM and 0.2% ethidium homodimer-1 in PBS), and cell viability was assessed using a fluorescence microscope (TE 2000, Nikon, Japan). WST-1 assay (EZ-3000 assay kit, DOGEN Daeil Lab Service, Seoul, Korea) was conducted to monitor the effect of MNP on HDFBs proliferation. Culture medium was aspirated and replaced with a diluted EZ-Cytox solution from the EZ-3000 assay (1:10 ratio) with growth medium. After incubation for 2 hrs at 37 °C, 100 μl of supernatant was collected and analyzed using a spectrometer at 440 nm. The remaining cells were replenished with fresh medium and continuously incubated for up to 3 days. The same concentration of EZ-Cytox solution with culture medium (1:10 mix) was used as a blank.

MNP Internalization Mechanism

We used chlorpromazine (CPZ) to investigate the uptake mechanism of MNP. HDFBs were re-suspended in 10 μg/ml CPZ in growth medium and cultured for 24 hrs, which was followed by exposure to MNP (2 $\mu g/cm^2$) for 8 hrs at 37 °C. Prussian blue and hematoxylin staining and an iron assay were then performed. We used the same cell lysate solution obtained from the 1% SDS buffer treatment for DNA assay. The DNA assay was conducted using a Quanti-iT™ PicoGreen® dsDNA assay kit (Invitrogen, Carlsbad, CA, USA) according to the manufacturer's procedure. The measured DNA contents of the MNP-treated group and non-treated group were presented relative to that of the MNP-treated group in both the CPZ-treated and non-treated groups, respectively.

Formation and Characterization of the 3-D Cellular Assembly

We magnetically induced a multi-layered HDFB structure by seeding at various concentrations on the confined area of a culture plate or PTFE film (Millipore, Billerica, MA, USA). First, the 24-well plate was coated with 20 μg/ml fibronectin in PBS for 2 hrs at 37 °C. A doughnut-shaped PDMS ring (1.5 mm in thickness, 15.5 mm in outer diameter, 6 mm in inner diameter) was then placed in the culture. A cylinder-shaped 3000 G neodymium magnet was placed underneath the culture plate. Trypsinized HDFBs from 1 to 5×10^5 cells/well suspended in a 500 μl volume of medium were seeded within the confined area, and the medium was changed after 4 hrs of incubation at 37 °C. Following 24 hrs of incubation, the samples were washed with PBS and fixed with 10% formalin solution or 4% paraformaldehyde for histological analysis or other processes, respectively.

The viability of magnetically assembled HDFBs with different density was observed using a LIVE/DEAD® assay. In addition, the DNA contents were measured after 1 day, and those from the group seeded with 1×10^5 magnetized cells cultured for up to 5 days were analyzed ($n = 4$) at day 1, 3, and 5. A multi-layered assembly was fixed with 10% formalin solution and dehydrated with graded EtOH (70–100%), xylene, and paraffin. Dehydrated samples in paraffin were hardened into a block for sectioning. Specimens were cut to 5 μm using a microtome (Shandon, Runcorn, Cheshire, UK). To perform H&E staining, sectioned sample slides were deparaffinized in xylene for 15 min and hydrated by dipping in 50% EtOH in xylene and graded EtOH (100–70%). The specimens were then treated with Harris hematoxylin and eosin solution. Slides were dehydrated by reverse hydration for 1 min and fixed with a 15 min xylene treatment. Slides were mounted with mounting medium (Richard-Allan Scientific, Kalamazoo, MI, USA). We observed these samples using optical microscopy (×400, $n = 5$). We used imaging software (NIS-Elements AR 3.0, Nikon, Japan) to measure the tissue thickness, presented as the average of 3 randomly selected points thickness on each staining image. For Prussian blue staining with nuclear fast red counterstaining, the samples were heated for 5 min at 60 °C in an oven and placed in xylene for 20 min for deparaffinization. Sample slides were hydrated in 50% EtOH in xylene and graded EtOH (100–70%).

For fluorescence staining for f-actin and nuclei, sample slides were fixed with 4% paraformaldehyde, permeabilized with a cytoskeleton buffer (CSK) (50 mM NaCl, 150 mM sucrose, 3 mM $MgCl_2$, 0.5% Triton-X, pH 6.8) for 20 min, and incubated with rhodamine-phalloidin for 1 hr. Following incubation, the samples were washed with PBS, mounted with a mounting medium that contained DAPI, and observed with fluorescence microscopy (×400, $n = 5$). The layer numbers of 3-D tissue were presented as an average from values of 3 fields that were randomly selected from each image.

Real-Time PCR

Three sample groups were used to analyze ECM expression and cell junction proteins using real-time PCR; the groups were seeded with 3×10^5 cells without MNP treatment, 3×10^5 and 5×10^5 of magnetized cells. mRNA of each assembly was extracted by using a Trizol reagent, and the concentration, purity, and integrity of the isolated mRNA were measured using a spectrophotometer (NANODROP 2000, Thermo Scientific, West Palm Beach, FL, USA). cDNA was synthesized with a thermal

cycler (Bio-Rad, Des Plaines, IL, USA) prepared by mixing mRNA (1 μg) and a Maxime RT Premix (Intron, Seoul, Korea) in a 20 μl reaction volume according to the manufacturer's instructions. Synthesized cDNA was used to perform real-time PCR using SYBR Premix Ex Taq (TAKARA, Otsu, Shiga, Japan) and StepOnePlus real-time PCR machine (Applied Biosystems, Forster city, CA, USA) for 40 cycles, melting at 95 °C for 15 sec, and annealing and extension at 60 °C for 60 sec for every primer set. The data obtained by real-time RT-PCR were analyzed using the comparative threshold cycle (Ct) method. The relative expression of each gene was calculated and compared to the expression level of GAPDH and subsequently normalized to the value for the 3×10^5 of un-magnetized cells seeded group. The method was performed in triplicate for each sample-gene match. The genes and related specific primers are as follows: GAPDH (RV: 5'-GGAAGGCCATGCCAGTGA-3', FW: 5'-CAAGGCTGTGGGCAAGGT-3') Collagen type I (RV: 5'-TAACCACTGCTCCACTCTGG-3', FW: 5'-GGACACAATGGATTGCAAGG-3') Collagen type IV (RV: 5'-GCATGGTACTGAAGCGACG-3', FW: 5'-CA CAGCCAGACAA CAGATGC-3'), Connexin 43 (RV: 5'-GTTTTGCTCACTTGCTTGCTTG-3', FW: 5'-TCCCCTCTCGCCT ATGTCTC-3'), Laminin (RV: 5'-GCAAACATCATCAA GTCAGCATT-3', FW: 5'-GAACTGCTAGAATTTACCTC CGC-3')

Immunofluorescence Staining

Sample slides were deparaffinized in xylene for 20 min and hydrated by dipping in 50% EtOH and graded EtOH (70–100%). After permeabilization, 50 μl of primary antibody (collagen type I and IV, laminin, connexin 43) diluted to 1:100 in blocking buffer (BB) was applied for 1 hr at 37 °C. After PBS wash, anti-rabbit IgG secondary Ab diluted to 1:100 in BB was applied for 1 hr at 37 °C. Sample slides were counterstained with a mounting medium containing DAPI and were washed with PBS and observed using fluorescence microscopy (×400, $n = 4$) and NIS-Elements AR 3.0.

Structural Control via Sequential Assembly

For labeling, HDFBs were treated for 1 hr with 0.5% of Vybrant®DiO (green) or Vybrant®DiD (red) labeling dye (Life Technologies, Carlsbad, CA, USA). Then, 2×10^5 cells of red-dye-labeled HDFBs were first seeded on the 24-well plate with 500 μl of medium. After 4 hrs, the medium was absorbed, and the same number of green-dye-labeled HDFBs in 500 μl medium were sequentially seeded, and then the process was repeated with red-labeled cells after an additional 4 hrs. We fixed sequentially assembled tissue with 4% paraformaldehyde. We observed z-plane stacked images of 3-D cellular assembly via confocal microscopy (Nikon A1, Japan) with a 1 μm interval between each plane (×400). The red coverage ratio was first measured with red signal intensity using NIS-Elements AR 3.0, and the green coverage ratio was determined as the non-red covered area. The green/red ratio was calculated by dividing the red coverage area into the green coverage area at each height.

Statistical Analysis

The quantitative values were expressed as mean ± standard deviation. The statistical significance was calculated using Student's t-test and ANOVA. When a p-value was less than 0.05, the result was considered statistically significant.

RESULTS

Interactions Between HDFBs and MNP

Figure 1 shows the schematic diagram of preparation of MNP and formation of 3-D cellular assembly. We first measured the effect of MNP concentration on their internalization into HDFBs over 24 hrs. As shown in Figure 2(a), the intensity, labeled by Prussian blue staining, increased as the treatment amount of MNP increased from 1 to 3 μg/cm^2. The stained images represented segregated MNP that appeared to overlap concomitantly with the image of counter-stained HDFBs. More aggregated MNP were observed in higher-concentration treatment groups. TEM analysis showed that MNP were entrapped within endosome-like vesicles when treated with 2 μg/cm^2 of HDFBs (Fig. 2(b)). The high-magnification TEM image revealed that particle size was approximately 10–20 nm (Fig. 2(c)). Most importantly, there was no indication of severe MNP clustering within the vesicle. The iron content proportionally increased as a function of MNP treatment amount, which was 24.81 ± 13.52, 34.40 ± 11.24, and 64.80 ± 15.84 pg/cell for MNP treatments at concentrations of 1, 2, and 3 μg/cm^2, respectively (Fig. 2(d)). The cytotoxicity of MNP was then evaluated via LIVE/DEAD assay. Figure 3(a) confirmed no cytotoxic effect of MNP on HDFBs for up to 3 μg/cm^2. In addition, HDFBs were

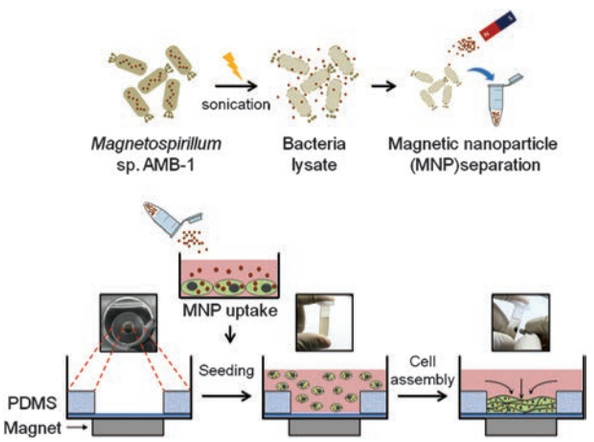

Figure 1. Schematic diagram of MNP preparation and 3-D cellular assembly using magnetized cells and magnetic force.

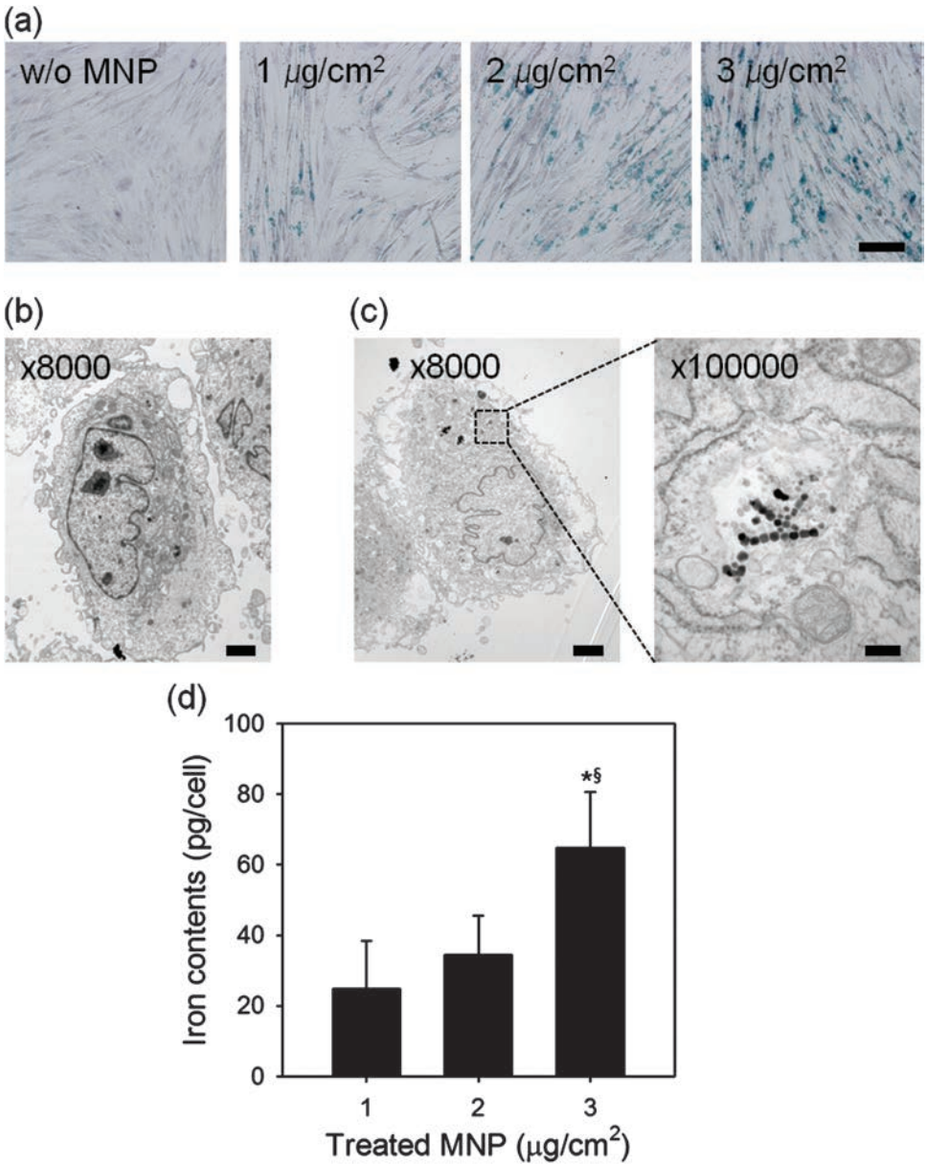

Figure 2. **Analysis of MNP internalization into HDFBs. (a) Prussian blue staining images of HDFBs that incorporated different amounts of MNP (scale bar = 100 μm). (b) TEM image of HDFBs without MNP treatment (scale bar = 2 μm). (c) TEM image of HDFBs treated with MNP (scale bar of left image = 5 μm, scale bar of right image = 200 nm). (d) Iron content in HDFBs treated with different amounts of MNP. ∗, § indicates statistical significance compared to the group treated with 1 and 2 μg/cm^2 ($p < 0.05$), respectively.**

continuously proliferating for over 3 days with the same rate as to the control despite MNP internalization. OD value of each group was similar, 1.7 ± 0.2, 11.9 ± 0.0, 1.9 ± 0.1, and 1.9 ± 0.1 at treatment levels of 0, 1, 2, and 3 μg/cm^2 of MNP, respectively, after one day of culture and the same trend was maintained over the 3 day culture period.

Mechanism of MNP Internalization

The MNP internalization mechanism in HDFBs was studied using CPZ. As shown in Figure 4, CPZ blocked internalization of MNP into HDFBs. The staining for Prussian blue became reduced when HDFBs were treated to MNP following exposure to CPZ. In contrast, robust internalization of MNP was re-confirmed for the group received MNP only (2 μg/cm^2). Treatment with CPZ exhibited minimal cytotoxicity to HDFBs; there were no deformities in cell morphology and similar levels of DNA were measured before and after treatment of MNP and CPZ as shown in Figure 4(c). The iron content that was internalized into HDFBs was 38.40 ± 5.09 pg/cell, which significantly decreased to 11.24 ± 2.92 pg/cell when endocytosis was blocked by CPZ.

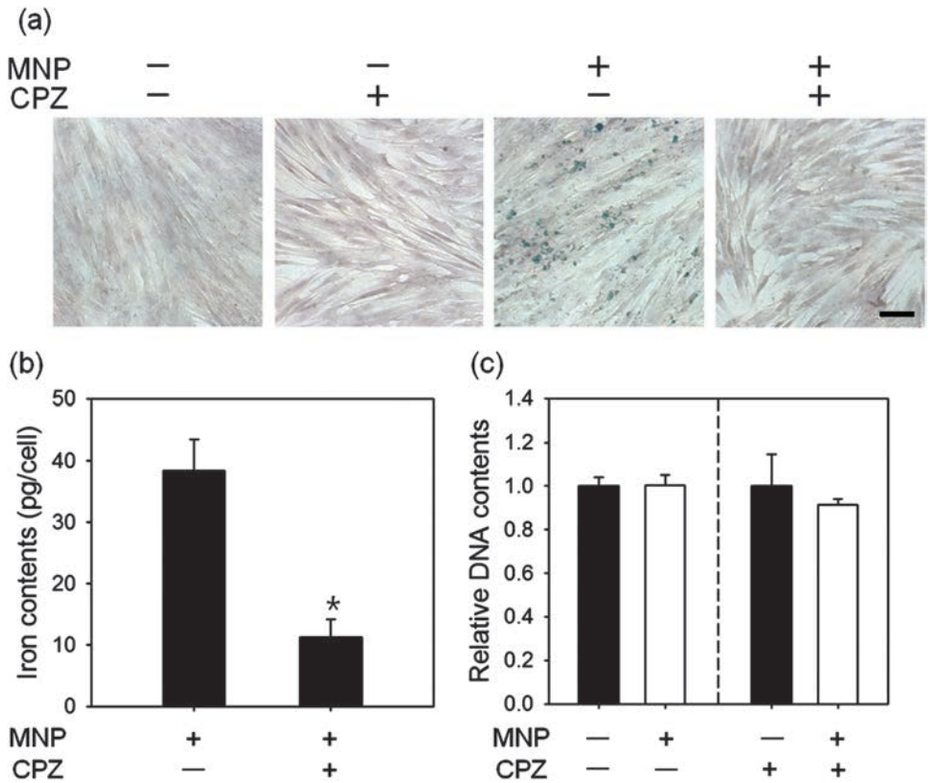

Figure 3. **Cytotoxicity of MNP on HDFBs. (a) Fluorescence images of HDFBs treated with different amounts of MNP, which were subsequently processed by LIVE/DEAD assay (scale bar = 100 μm). (b) Effect of various MNP amounts on the proliferation of HDFBs analyzed by WST-1 assay. ∗, §, # indicates statistical significance compared to the group of without MNP on day 1, 2, 3 ($p < 0.05$), respectively.**

3-D Cellular Assembly

We then examined the effect of seeding density on magnetically-assisted 3-D HDFB assembly. Despite extremely high seeding, live cell signals were predominantly observed with a few negligible red signals in the assembled cell construct (Fig. 5(a)). The green signal became more intense and brighter with increasing cell numbers. Meanwhile, accumulation of MNP within assembled 3-D tissue was identified by dark blotches where the seeding density increased. As shown in Figure 5(b), the DNA content of MNP-treated HDFBs assembly proportionally increased as a function of seeding density up to 5×10^5. In contrast, the value was significantly lower for HDFBs without MNP treatment and reached a plateau after seeding with 4×10^5 cells. For example, the DNA content increased to 2503.04 ± 127.70 ng/well for groups treated with 5×10^5 magnetized cells while it was only 1055.33 ± 52.58 ng/well for the group seeded with 5×10^5 of non-magnetized HDFBs. The difference in DNA content between the magnetized and non-magnetized groups increased with seeding density. In addition, the DNA content of the 3-D assembled cell construct increased from 699.26 ± 36.97 on 1 day to 1088.23 ± 22.87 on 5 day.

H&E staining showed that the assembly increased with respect to cell numbers (Fig. 6(a)). We observed a uniform distribution of violet-colored nuclei throughout the 3-D tissue and dark spots of localized MNP. Prussian blue staining showed homogeneous blue signals with samples that received 1, 2, and 3×10^5 magnetized cells. However, when higher seeding densities were used (4 and 5×10^5 cells), magnetized cells diffusely distributed and yielded large clusters preferentially at the bottom of the assembled structure. These results imply that MNP were favorably forced to move toward the bottom during cellular assembly due to application of the strong magnetic force. The thickness and number of stratified nuclei increased with seeding density, although the control group, seeded with 5×10^5 cells, only had a single layer (Figs. 6(b)–(d)). The number of stratified nuclei was 2.2 ± 0.9, which increased up to 9.3 ± 1.6 with the thickness of 41.90 ± 1.69 m as the seeding density varied from 1 to 5×10^5. The increasing trend of thickness and stratified nuclei number was consistent with that of the DNA assay.

Expression of ECM and Junction Proteins Within 3-D Cellular Assembly

We then compared gene expressions of key ECM and cell-junction proteins in 3-D assembly to 2-D cultured cells through real-time PCR. As shown in Figure 7(a), 3-D

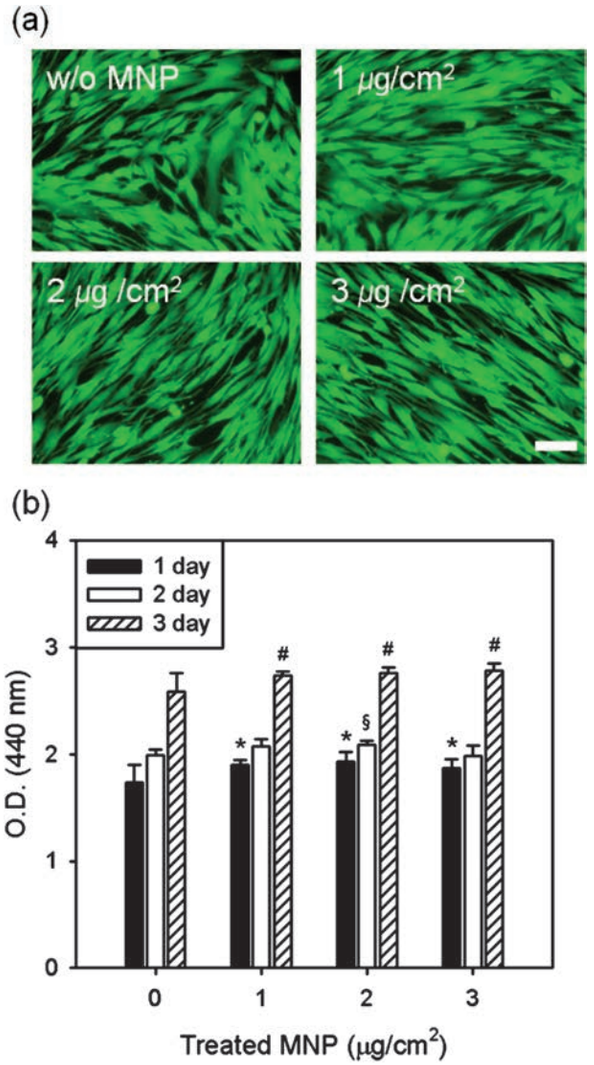

Figure 4. **Elucidation of the potential underlying internalization mechanism of MNP into HDFBs. (a) Prussian blue staining images of HDFBs after MNP treatment with and without CPZ conditioning (scale bar = 100 μm). (b) Comparison of iron content in HDFBs after MNP treatment with and without CPZ conditioning. * indicates statistical significance compared to the group of without CPZ conditioning ($p < 0.05$). (c) Relative DNA from HDFBs after MNP treatment with and without CPZ conditioning.**

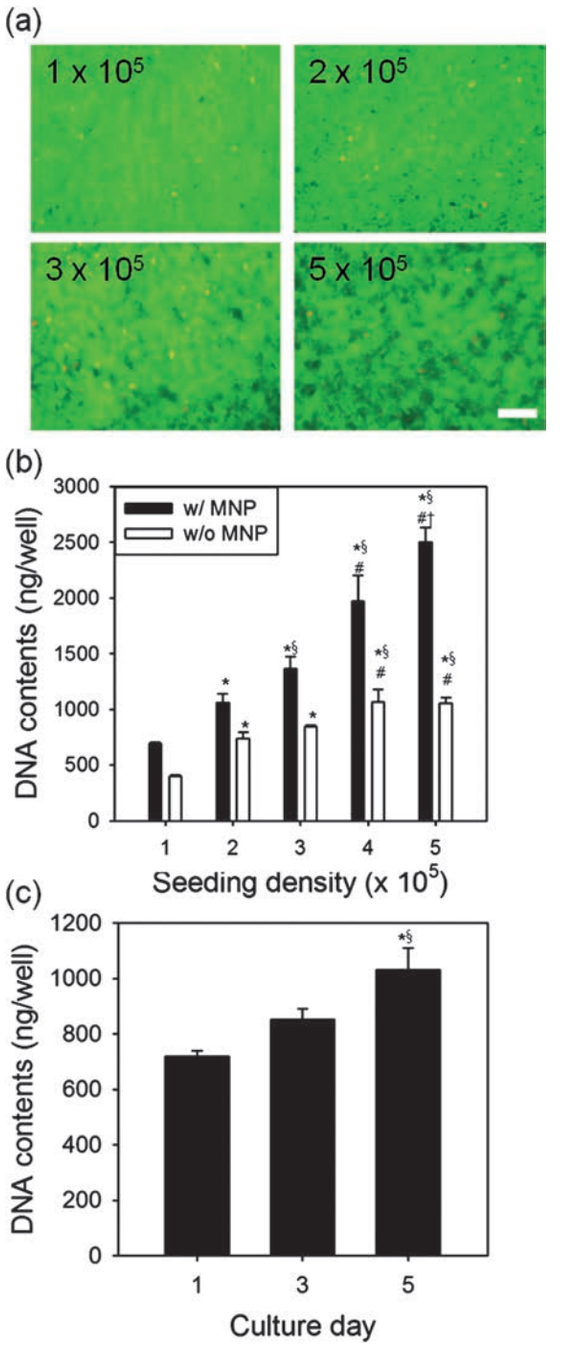

Figure 5. **Fabrication of magnetically-assisted cellular assembly. (a) Fluorescence images of 3-D cellular assembly fabricated with different cell numbers ranging from 1 to 5×10^5 cells (scale bar = 100 μm), which were processed by LIVE/DEAD assay. (b) DNA content of HDFBs constructed as 3-D cellular assembly of magnetized cells by MNP treatment and 2-D culture control. ∗, §, #, and † indicate statistical significance compared to that from the 1, 2, 3 and 4×10^5 cells seeded groups, respectively ($p < 0.05$). (c) DNA content of the 3-D assembled construct that was seeded with 1×10^5 magnetized cells and cultured over 5 days on tissue culture plate. ∗, § indicates significance compared to the value of the 1 and 3 day culture group ($p < 0.05$), respectively.**

assembly formed with 3 and 5×10^5 cells showed significantly lower expression of collagen type I and type IV than 2-D culture. In contrast, connexin 43, which is involved in cell to cell junctions, was strongly expressed within 3-D assembly compared to 2-D cultured cells, with the expression of connexin 43 being 1.26 ± 0.12- and 1.17 ± 0.04-fold greater for the group seeded with 3 and 5×10^5 magnetized cells compared to that seeded with 3×10^5 non-magnetized cells. This difference was statistically significant. In addition, the relative expression of laminin was significantly greater for the 5×10^5 cell-seeded group.

Immunofluorescence staining was then performed and directed toward the same proteins tested for PCR. As shown in Figure 7(b), target proteins were homogenously distributed within the 3-D structure.

Hierarchical Structure of 3-D Cellular Assembly

Finally, we fabricated a 3-D hierarchical structure by serial repetition of magnetically-assisted assembly process with 2×10^5 magnetized cells. As shown in Figure 8(a), f-actin stress fibers were isotropically distributed in the 3-D assembly. The thickness visualized by control microscopy was approximately 25 μm. The side view demonstrated more intensified blue fluorescence versus red near the 3-D assembly surface, indicating that stress fiber formation may be heterogeneously controlled by the thickness. HDFBs pre-labeled with red and green dyes revealed close apposition of the middle layer with green fluorescence to the bottom and top layers of HDFBs labeled as red, in which three clearly distinguishable layers were displayed (Fig. 8(a)). Images taken from different heights demonstrated different color distributions; red fluorescence exclusively appeared at the heights of 4 μm and 18 μm, while the green signal was dominant at 12 μm (Fig. 8(c)). We measured the coverage area of each fluorescence and calculated the ratio of green/red by analyzing the xy plane through images taken from different heights. As shown in Figure 8(d), the red fluorescence covered almost 100% of the xy plane at 0 to 4 μm heights. However, the green signal moderately increased from 4 μm and reached the highest value of 63.77% at 12 μm. The green signal coverage area gradually decreased to about 1.18% until 20 μm. The red signal increased from 12 μm and reached 98.82% at 20 μm. In addition, the ratio of green/red signal also increased until 12 μm, where it measured 1.76.

DISCUSSION

Interactions Between HDFBs and MNP

Although many studies reported the use of MNP for 3-D cellular assembly as a platform for drug screening or as a functional tissue in regenerative medicine, there

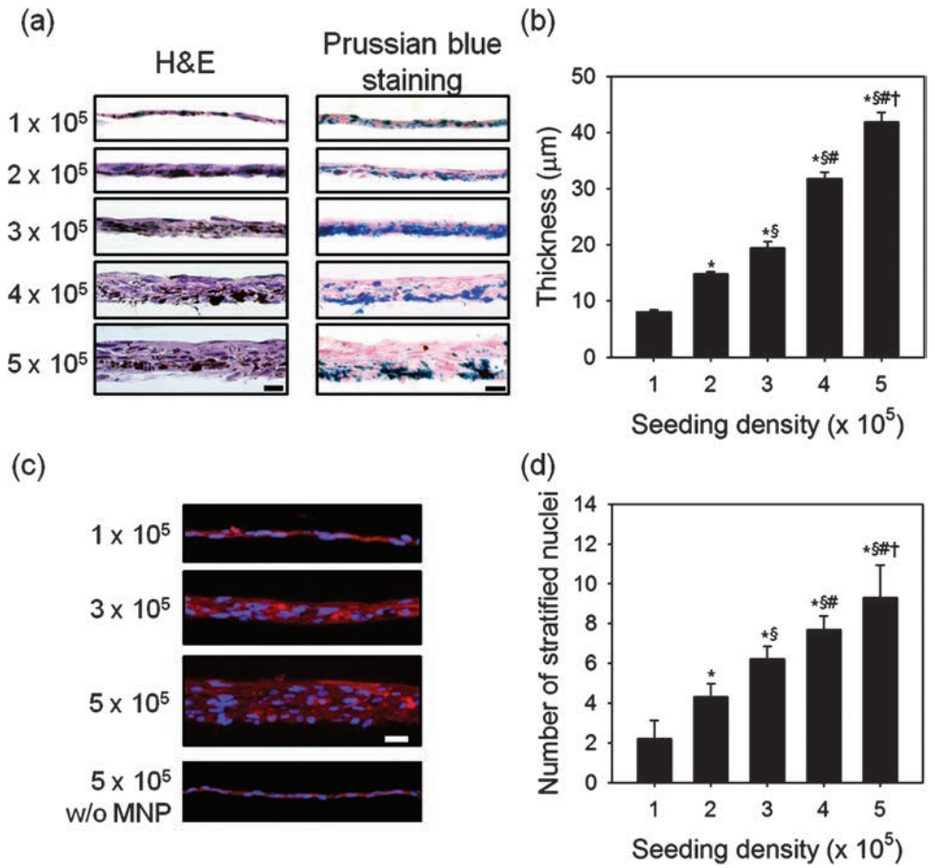

Figure 6. **Structural analysis of 3-D assemblies formed using different cell numbers. (a) H&E and Prussian blue staining images of the section of the assembly (scale bar = 20 μm). (b) Thickness measurement conducted by sectional image analysis. ∗, §, #, and † indicate statistical significance compared to the 1, 2, 3 and 4 x 10^5 cells seed groups ($p < 0.05$), respectively. (c) Fluorescence images of the 3-D assembly stained for f-actin and nuclei (scale bar = 20 μm). (d) Measurement of stratified nuclei number according to cell number. ∗, §, #, and † indicate statistical significance compared to the 1, 2, 3 and 4 x 10^5 cell seeding groups ($p < 0.05$), respectively.**

remain some technical issues for the achievement of homogeneously magnetized cells.[14, 18] For example, magnetite cationic liposome (MCL) presented various particle sizes, which required rigorous purification steps for effective internalization into cells (optimal size of approximately 150 nm).[18] Small fragments of the hydrogel-magnetic iron oxide (MIO) complex can be internalized in the cytoplasm, but those with the larger size remained at the cell surface.[14] In this study, MNP isolated from bacteria demonstrated stable incorporation into HDFBs, controlled by change in the MNP concentration (Fig. 2(d)). Magnetization of cells may be dependent on the amount of internalized MNP and must be sufficient for magnetic attraction. In order to facilitate the internalization of MNP to the target cells, MNP were modified with functional molecules such as poly-L-lysine, heparin, dextran coating, and positive liposome.[23, 24] As compared to previous work, the MNP used in this study appeared to be well delivered and dispersed in the cytoplasm of HDFBs. These results may be partially attributable to the presence of phospholipid layer surrounding the MNP surface, which was reported to induce efficient internalization via binding to cell membrane.[24, 25] In addition, the negative charge of the cell membrane might improve MNP dispersion by preventing aggregation. We also demonstrated that the bacteria-derived MNP did not exhibit cytotoxicity on HDFBs (Fig. 4). The non-cytotoxic effect of the same type of MNP has been reported in previous studies that used other cell types of endothelial progenitor cells and hMSCs.[22, 25] Collectively, these results support that HDFBs can be magnetized by controlled amounts of MNP treatment without compromising cellular activity.

Potential MNP Internalization Mechanism

Solid particles and extracellular fluid are naturally absorbed by cells via endocytosis that can be categorized into phagocytosis and pinocytosis.[23] Vesicles with a diameter of 0.5–10 μm enter the cells via phagocytosis, while smaller vesicles are internalized by pinocytosis, which was anticipated to be the main mechanism for our prepared MNP, considering their approximately 20–30 nm sizes. Pinocytosis may be mediated by two distinct pathways. Langston Suen et al. used gold nanoparticles with sizes of 50, 120, and 250 nm and found that the nanoparticle size influenced internalization into the cell cytoplasm; nanoparticles of 50 nm entered into cells via clathrin-mediated endocytosis, while nanoparticles of 250 nm entered into cells via clathrin-independent endocytosis.[26] We used CPZ, which inhibits clathrin-mediated endocytosis, by crosslinking the receptor to confirm the mechanism of MNP uptake. The CPZ treatment decreased incorporation of MNP, suggesting that MNP uptake is mainly regulated by clathrin-mediated endocytosis (Figure 3). In addition to nanoparticle size, other factors including shape, charge, and hydrophobicity are known to affect cellular internalization. Previous characterization of MNP derived from

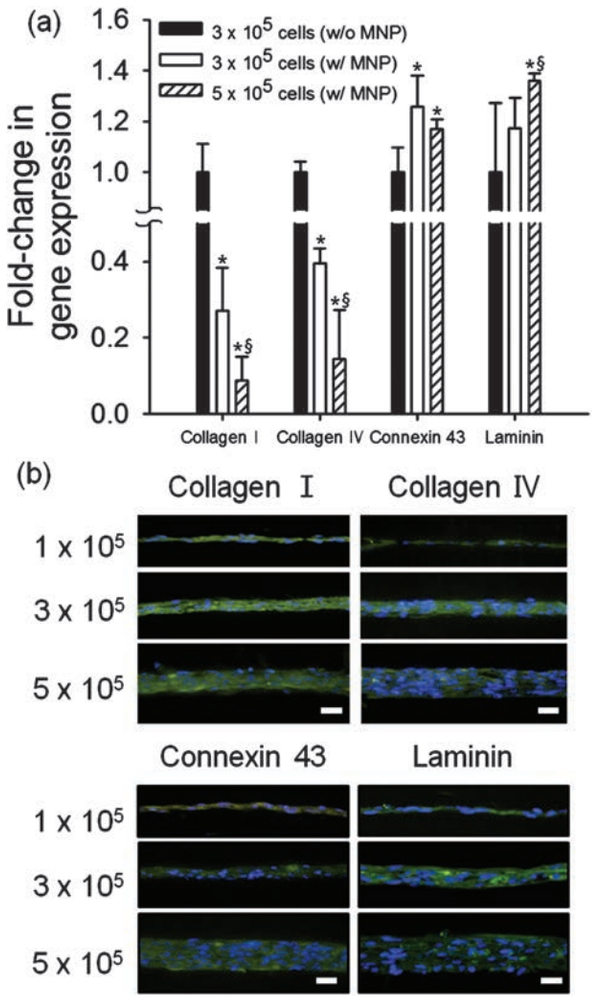

Figure 7. Expression of ECM and cell junction proteins of 3-D cellular assembly. (a) Fold-change in gene expression of collagen type I, collagen type IV, connexin 43, and laminin. ∗, § indicates statistical significance compared to the control group seeded with 3×10^5 cells without and with MNP treatment ($p < 0.05$), respectively. (b) Immunofluorescence staining images of proteins (scale bar = 20 μm).

the same bacterial strain revealed that the particle surface was coated with phospholipid and was negatively charge.[23] Although anionic particles are likely internalized into cells via the clathrin-independent pathway, we speculate that the combination of the small size and anionic nature of MNP may have promoted clathrin-mediated endocytosis.

3-D Cellular Magnetically-Assisted Assembly

LIVE/DEAD assay results from magnetically assembled cellular constructs showed that the process was not detrimental to cell viability (Fig. 5(a)). In addition, the DNA contents of the fabricated cellular assembly steadily increased with cell seeding density, whereas the DNA content reached a plateau in 2-D culture. Conventionally, cells cultured in a 2-D environment undergo arrested

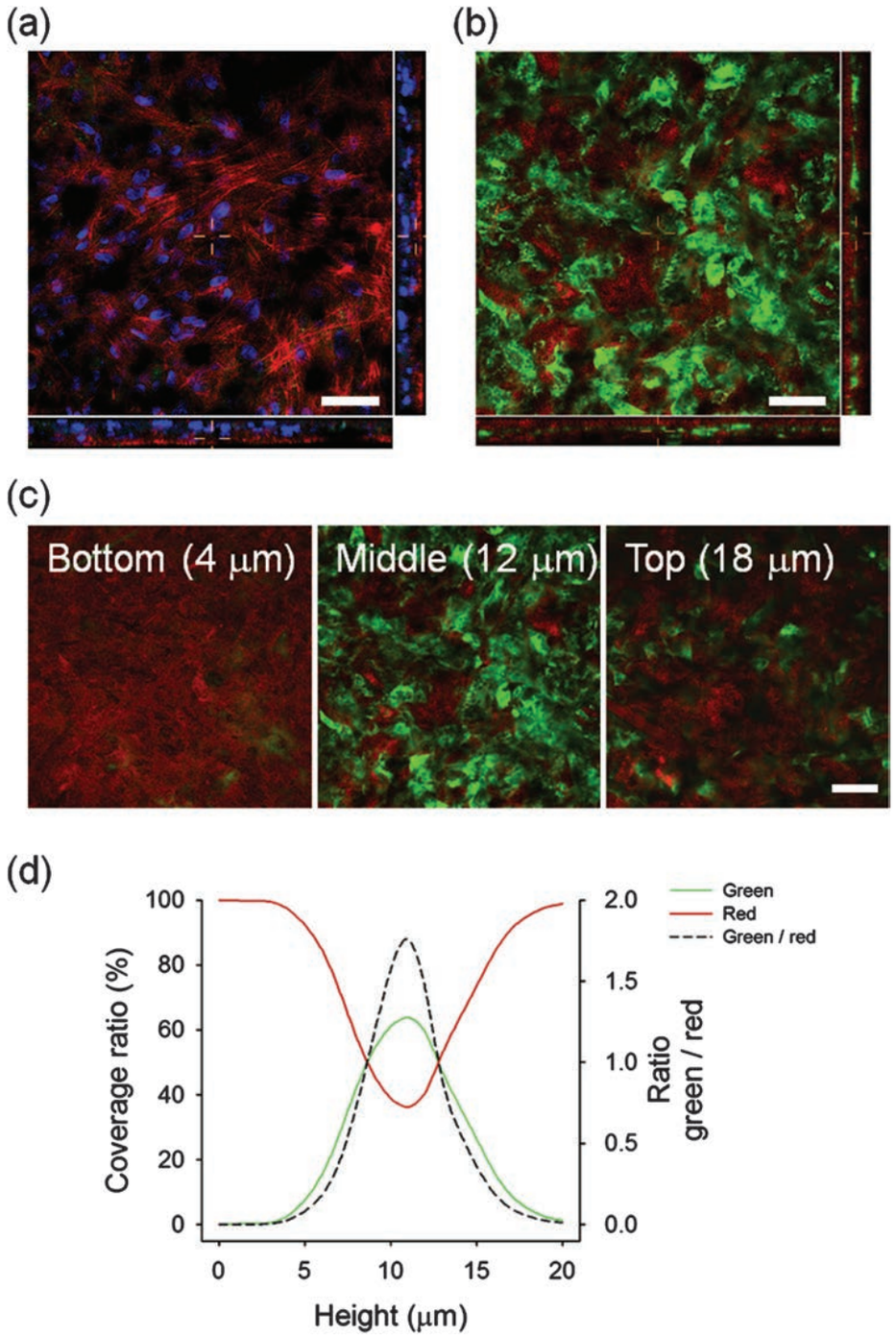

Figure 8. **Modulation of hierarchical structure of 3-D cellular assembly. (a) Image of serially stacked tissue visualized for nuclei and f-actin (scale bar = 50 μm). (b) Confocal microscope image of 3-D cellular assembly serially stacked with HDFBs pre-labeled with different dyes and (c) representative orthogonal images at different planes (bottom: 4 μm, middle: 12 μm, top: 18 μm) (scale bar = 50 μm). (d) Measurement of coverage ratio of green and red signals and green/red signal ratio according to 3-D assembled tissue height.**

proliferation after forming a monolayer in a limited area, which made it difficult to form a multi-layered cellular assembly.[27] In contrast, our results suggest that a large number of magnetized cells can be stacked to form a larger cellular assembly. We also confirmed that magnetized cells can proliferate over 5 days of culture following the magnetic assembly process. DNA content at day 5 increased to 1.56 times the amount relative to the value at day 1

(Fig. 5(c)). The proliferation of magnetically assembled cells in this study is lower than a previous study that assessed spheroids fabricated by magnetic levitation.[14] In our system, the magnetized cells are attracted to the confined area for cellular assembly, limiting the spatial freedom for cell proliferation, which may have contributed to the overall low proliferation rate of cells.

Prussian blue staining showed a more concentrated distribution of blue signal on the bottom of the cellular assembly, which could represent a stronger MNP attraction to the magnet at the interface. Attraction of MNP using a magnet has been used for targeted drug delivery, and the results presented localized MNP signals near the magnet's position.[28] Most importantly, the cellular assembly thickness increased with cell number, suggesting that cell number is an important parameter that affects the volume of engineered 3-D tissue formation (Fig. 6). These results are consistent with previous reports showing that strong deriving forces such as a magnet or ECM-based interactions that enable cellular assembly are required to form a 3-D structure that has a thickness proportionally regulated by cell number.[10, 29] It was also evident that the thickness of 3-D assembled cells is dependent on the process, in which the thickness of 3-D multiple-layered assembly prepared from our system seems to be lower than that fabricated from cell accumulation technique. In the cell accumulation approach, a layer-by-layer film of fibronectin and gelatin is alternatively deposited on the surface of cells by repeated coating of each protein, which can attract cells for assembly and contribute to the overall thickness.[10] The assembled cells are, in principle, attached through cell-ECM binding, which may result in a slightly greater thickness of assembled 3-D tissue as compared to those of magnetically assembled structure. Although ECM coating on the surface of cells generates stable cellular assembly, the overall layer-by-layer process takes a few hours, and a large number of cells can be lost due to repeated centrifugation and mechanical disaggregation of cells. Therefore, cellular assembly by magnetized cells can create a reproducible multiple-layered structure that can be assembled with simpler steps under milder experimental conditions than the cell accumulation technique and cell sheet engineering.

ECM and Junction Protein Expression Within the 3-D Cellular Assembly

The natural cellular microenvironment is hierarchically formed by complex interactions of cells with the ECM and other neighboring cells. ECM is secreted by cells and provides a structural and mechanical framework in which cell-ECM interactions mediate numerous biological phenomenon such as cell adhesion, proliferation, differentiation, and death.[30] Meanwhile, cell-cell contact is controlled by binding between cell surface receptors, which is implicated in cell mechanics, migration, and survival. Despite many reports on 3-D cell assembly methods, few studies have investigated the expression of ECM and junction proteins. We observed a decrease in the expression levels of collagen type I and IV from 3-D cellular assembly compared with results from 2-D culture (Fig. 6(a)). These results are similar to a report by Tseng et al., demonstrating decreased expression of collagen I and laminin from 3-D assembled magnetized human umbilical vein endothelial cells (HUVECs) compared to cells cultured on TCP.[31] They observed evenly distributed collagen I and laminin through a vertically sectioned view of the assembled cells, similar to our findings shown in Figure 6(b). We speculate that the expression level may be affected by the mechanical property of environment. Studies of the relationship between the expression of ECM molecules and stiffness of the surrounding environment showed that laminin expression in epithelial cells increased in the stiffer environment compared with the softer environment.[32] Therefore, the expression level could have decreased since cells in 3-D assembly are directly exposed to the cell layer, which is softer than the culture dish. Interestingly, we observed an increase in connexin 43 expression based on PCR results and an even distribution of the protein on the sectional view. Connexin 43 staining from cardiomyocyte spheroids also indicated an increased signal compared with the 2-D culture conditions.[33] Increase in connexin 43 expression in the 3-D assembly might be caused by compactly formed cell-cell junctions, since connexin 43 is known to be localized at tight junctions to form tight binding between cells and ensure ECM-cell binding.[34] Collectively, our results revealed that a magnetically-assisted cellular assembly is formed by homogeneously distributed structural ECM proteins and strengthened cell-cell interactions.

Most natural tissues exhibit distinguishable 3-Dstructures of the assembled cell and ECM, which regulate their function. Hence, mimicking the sophisticated structure has been challenging for 3-D cellular assembly techniques.[35] We performed serial assembly to fabricate 3-D tissue with clearly observable layers with compact and stacked f-actin stress fiber formation. Similarly, hepatocyte spheroids with a 50 μm diameter also exhibited dense and piled f-actin structures.[36] The ratio metric analysis of the present study confirmed minimal diffusive migration of cells during the assembly process. The discernible layers in Figures 8[b and c] demonstrate the feasibility of this magnetically-assisted assembly technique for constructing 3-D cellular structures. Serial assembly of 3-D structures has been conducted via various methods including cell sheet engineering, cell accumulation, and 3-D printing.[10, 37, 38] Previous works with magnetized cells also presented ideas for creating several forms of tissue such as tubular and layered structures.[39, 40] Similarly, our results showed the possibility of fine control and fabrication of 3-D cellular assembly, suggesting that assembling different types of cells via the developed system will be a powerful tool for achieving ex vivo tissue formation.

CONCLUSION

In this study, we developed multi-layered 3-D cell assembly using magnetized cells and magnetic force, and assessed the structure-oriented cell-cell/cell-ECM interactions. The amount of incorporated MNP increased as the increase in MNP treatment amount up to 3 $\mu g/cm^2$. TEM analysis revealed that MNP were entrapped within vesicle-like structures in the cytoplasm, which appeared to be mediated by clathrin-mediated endocytosis. The LIVE/DEAD assay and WST-1 assay indicated that MNP did not have adverse effects on cell viability or proliferation within the range (1 to 3 $\mu g/cm^2$) tested. As cell number increased, the DNA content steadily increased to form multi-layered structure with magnetized cells; however, the cells without MNP treatment were unable to form such a structure regardless of seeding density. Magnetically-assembled cells presented a favorable environment for cells, demonstrating proliferative activity over 5 days. Sectional analysis showed increasing thickness and stratified nuclei number proportionate to the seeded cell number. Immunofluorescence staining of ECM molecules presented evenly distributed signals, and different expression levels of collagen type I and IV were observed in 3-D assembly compared to 2-D culture conditions. We then used serial assembly to fabricate 3-D assembly with a complicated structure composed of three distinguishable layers. In conclusion, the developed assembly technique is a promising option for fabricating 3-D engineered tissue that mimic the ECM structure and cell-cell junction of natural tissue.

Acknowledgment: This work was supported by a National Research Foundation of Korea (NRF) funded by the the Ministry of Science, ICT and Future Planning (NRF-2013R1A2A2A03067809) and Radiation Technology R&D program (NRF-2015M2A2A6021052).

REFERENCES

1. M. A. Schwartz, Integrins and extracellular matrix in mechanotransduction. *Cold Spring Harb. Perspect. Biol.* 2, a005066 (**2010**).
2. K. M. Yamada and E. Cukierman, Modeling tissue morphogenesis and cancer in 3D. *Cell.* 130, 601 (**2007**).
3. S. F. Badylak, D. O. Freytes, and T. W. Gilbert, Extracellular matrix as a biological scaffold material: Structure and function. *Acta Biomater.* 5, 1 (**2009**).
4. L. G. Griffith and M. A. Swartz, Capturing complex 3D tissue physiology *in vitro*. *Nat. Rev. Mol. Cell. Bio.* 7, 211 (**2006**).
5. J. Shi, A. R. Votruba, O. C. Farokhzad, and R. Langer, Nanotechnology in drug delivery and tissue engineering: From discovery to applications. *Nano Lett.* 10, 3223 (**2010**).
6. D. L. Elbert, Bottom-up tissue engineering. *Curr. Opin. Biotech.* 22, 674 (**2011**).
7. A. I. Neto, C. R. Correia, M. B. Oliveira, M. I. Rial-Hermida, C. Alvarez-Lorenzo, R. L. Reis, and J. F. Mano, A novel hanging spherical drop system for the generation of cellular spheroids and high throughput combinatorial drug screening. *Biomat. Sci.* 3, 581 (**2015**).
8. E. Fennema, N. Rivron, J. Rouwkema, C. V. Blitterswijk, and J. D. Boer, Spheroid culture as a tool for creating 3D complex tissues. *Trends Biotechnol.* 31, 108 (**2013**).
9. I. Elloumi-Hannachi, M. Yamato, and T. Okano, Cell sheet engineering: A unique nanotechnology for scaffold-free tissue reconstruction with clinical applications in regenerative medicine. *J. Intern. Med.* 267, 54 (**2010**).
10. A. Nishiguchi, H. Yoshida, M. Matsusaki, and M. Akashi, Rapid construction of three-dimensional multilayered tissues with endothelial tube networks by the cell-accumulation technique. *Adv. Mater.* 23, 3506 (**2011**).
11. E. A. Lee, H. Yim, J. Heo, H. Kim, G. Jung, and N. S. Hwang, Application of magnetic nanoparticle for controlled tissue assembly and tissue engineering. *Arc. Pharm. Res.* 37, 120 (**2014**).
12. A. Ito, E. Hibino, C. Kobayashi, H. Terasaki, H. Kagami, M. Ueda, T. Kobayashi, and H. Honda, Construction and delivery of tissue-engineered human retinal pigment epithelial cell sheets, using magnetite nanoparticles and magnetic force. *Tissue Eng.* 11, 489 (**2005**).
13. D. M. Timm, J. Chen, D. Sing, J. A. Gage, W. L. Haisler, S. K. Neeley, R. M. Raphael, M. Dehghani, K. P. Rosenblatt, T. C. Killian, H. Tseng, and G. R. Souza, A high-throughput three-dimensional cell migration assay for toxicity screening with mobile device-based macroscopic image analysis. *Sci. Rep.* 3, 3000 (**2013**).
14. G. R. Souza, J. R. Molina, R. M. Raphael, M. G. Ozawa, D. J. Stark, C. S. Levin, L. F. Bronk, J. S. Ananta, J. Mandelin, M. M. Georgescu, J. A. Bankson, J. G. Gelovani, T. C. Killian, W. Arap, and R. Pasqualini, Three-dimensional tissue culture based on magnetic cell levitation. *Nat. Nanotechnol.* 5, 291 (**2010**).
15. A. Ito, K. Ino, M. Hayashida, T. Kobayashi, H. Matsunuma, H. Kagami, M. Ueda, and H. Honda, Novel methodology for fabrication of tissue-engineered tubular constructs using magnetite nanoparticles and magnetic force. *Tissue Eng.* 11, 1553 (**2005**).
16. A. C. Daquinag, G. R. Souza, and M. G. Kolonin, Adipose tissue engineering in three-dimensional levitation tissue culture system based on magnetic nanoparticles. *Tissue Eng. Part C-Me.* 19, 336 (**2013**).
17. A. Ito, M. Hayashida, H. Honda, K. I. Hata, H. Kagami, M. Ueda, and T. Kobayashi, Construction and harvest of multilayered keratinocyte sheets using magnetite nanoparticles and magnetic force. *Tissue Eng.* 10, 873 (**2004**).
18. K. Shimizu, A. Ito, T. Yoshida, Y. Yamada, M. Ueda, and H. Honda, Bone tissue engineering with human mesenchymal stem cell sheets constructed using magnetite nanoparticles and magnetic force. *J. Biomed. Mater. Res. B* 82B, 471 (**2007**).
19. T. Kito, R. Shibata, M. Ishii, H. Suzuki, T. Himeno, Y. Kataoka, Y. Yamamura, T. Yamamoto, N. Nishio, S. Ito, Y. Numaguchi, T. Tanigawa, J. K. Yamashita, N. Ouchi, H. Honda, K. Isobe, and T. Murohara, iPS cell sheets created by a novel magnetite tissue engineering method for reparative angiogenesis. *Sci. Rep.* 3, 1418 (**2013**).
20. H. Akiyama, A. Ito, Y. Kawabe, and M. Kamihira, Fabrication of complex three-dimensional tissue architectures using a magnetic force-based cell patterning technique. *Biomed. Microdevices* 11, 713 (**2009**).
21. S. Seong and T. H. Park, Swimming characteristics of magnetic bacterium, Magnetospirillum sp. AMB-1, and implications as toxicity measurement. *Biotechnol. Bioeng.* 76, 11 (**2001**).
22. J. A. Kim, J. H. Choi, M. Kim, W. J. Rhee, B. Son, H. K. Jung, and T. H. Park, High-throughput generation of spheroids using magnetic nanoparticles for three-dimensional cell culture. *Biomaterials* 34, 8555 (**2013**).
23. L. Kou, J. Sun, Y. Zhai, and Z. He, The endocytosis and intracellular fate of nanomedicines: Implication for rational design. *Asian J. Pharm. Sciences* 8, 1 (**2013**).
24. J.-h. Lee, M. J. Jung, Y. H. Hwang, Y. J. Lee, S. Lee, D. Y. Lee, and H. Shin, Heparin-coated superparamagnetic iron oxide for *in vivo* MR imaging of human MSCs. *Biomaterials* 33, 4861 (**2012**).
25. J. Kim, H. Lee, H.-J. Kang, and T. Park, The targeting of endothelial progenitor cells to a specific location within a microfluidic channel using magnetic nanoparticles. *Biomed. Microdevices* 11, 287 (**2009**).

26. W. L. Langston Suen, and Y. Chau, Size-dependent internalisation of folate-decorated nanoparticles via the pathways of clathrin and caveolae-mediated endocytosis in ARPE-19 cells. *J. Pharm. Pharmacol.* 66, 564 **(2014)**.
27. A. Puliafito, L. Hufnagel, P. Neveu, S. Streichan, A. Sigal, D. K. Fygenson, and B. I. Shraiman, Collective and single cell behavior in epithelial contact inhibition. *Proc. Natl. Acad. Sci. U S A* 109, 739 **(2012)**.
28. C. Alexiou, W. Arnold, P. Hulin, R. J. Klein, H. Renz, F. G. Parak, C. Bergemann, and A. S. Lubbe, Magnetic mitoxantrone nanoparticle detection by histology, X-ray and MRI after magnetic tumor targeting. *J. Magn. Magn. Mater.* 225, 187 **(2001)**.
29. G. Frasca, F. Gazeau, and C. Wilhelm, Formation of a three-dimensional multicellular assembly using magnetic patterning. *Langmuir* 25, 2348 **(2009)**.
30. S. H. Kim, J. Turnbull, and S. Guimond, Extracellular matrix and cell signalling: The dynamic cooperation of integrin, proteoglycan and growth factor receptor. *J. Endocrinol.* 209, 139 **(2011)**.
31. H. Tseng, L. R. Balaoing, B. Grigoryan, R. M. Raphael, T. C. Killian, G. R. Souza, and K. J. Grande-Allen, A three-dimensional co-culture model of the aortic valve using magnetic levitation. *Acta Biomater.* 10, 173 **(2014)**.
32. J. L. Eisenberg, A. Safi, X. Wei, H. D. Espinosa, G. S. Budinger, D. Takawira, S. B. Hopkinson, and J. C. Jones, Substrate stiffness regulates extracellular matrix deposition by alveolar epithelial cells. *Res. Rep. Biol.* 2011, 1 **(2011)**.
33. B. R. Desroches, P. Zhang, B. R. Choi, M. E. King, A. E. Maldonado, W. Li, A. Rago, G. Liu, N. Nath, K. M. Hartmann, B. Yang, G. Koren, J. R. Morgan, and U. Mende, Functional scaffold-free 3-D cardiac microtissues: A novel model for the investigation of heart cells. *Am. J. Physiol. Heart Circ. Physiol.* 302, H2031 **(2012)**.
34. H. W. Ai, M. A. Baird, Y. Shen, M. W. Davidson, and R. E. Campbell, Engineering and characterizing monomeric fluorescent proteins for live-cell imaging applications. *Nat. Protoc.* 9, 910 **(2014)**.
35. T. L. Lu, Y. H. Li, and T. Chen, Techniques for fabrication and construction of three-dimensional scaffolds for tissue engineering. *Int. J. Nanomed.* 8, 337 **(2013)**.
36. D. Y. No, S. A. Lee, Y. Y. Choi, D. Park, J. Y. Jang, D. S. Kim, and S. H. Lee, Functional 3D human primary hepatocyte spheroids made by co-culturing hepatocytes from partial hepatectomy specimens and human adipose-derived stem cells. *Plos One*. 7, e50723 **(2012)**.
37. Y. Haraguchi, T. Shimizu, T. Sasagawa, H. Sekine, K. Sakaguchi, T. Kikuchi, W. Sekine, S. Sekiya, M. Yamato, M. Umezu, and T. Okano, Fabrication of functional three-dimensional tissues by stacking cell sheets *in vitro*. *Nat. Protoc.* 7, 850 **(2012)**.
38. F. Pati, J. Jang, D. H. Ha, S. W. Kim, J. W. Rhie, J. H. Shim, D. H. Kim, and D. W. Cho, Printing three-dimensional tissue analogues with decellularized extracellular matrix bioink. *Nat. Commun.* 5, 3935 **(2014)**.
39. H. Tseng, J. A. Gage, R. M. Raphael, R. H. Moore, T. C. Killian, K. J. Grande-Allen, and G. R. Souza, Assembly of a three-dimensional multitype bronchiole coculture model using magnetic levitation. *Tissue Eng. Part C-Me*. 19, 665 **(2013)**.
40. K. Shimizu, A. Ito, M. Arinobe, Y. Murase, Y. Iwata, Y. Narita, H. Kagami, M. Ueda, and H. Honda, Effective cell-seeding technique using magnetite nanoparticles and magnetic force onto decellularized blood vessels for vascular tissue engineering. *J. Biosci. Bioeng.* 103, 472 **(2007)**.